PAni-coated LiFePO$_4$ Synthesized by a Low Temperature Solvothermal Method

Wélique Silva Fagundes[a], Farlon Felipe Silva Xavier[a], Laiane Kalita Santana[a], Matheus Ezequiel

Azevedo[a], Sheila Cristina Canobre[a], Fábio Augusto Amaral[a]*

[a]Laboratório de Armazenamento de Energia e Tratamento de Efluentes - LAETE, Instituto de Quimíca,
Universidade Federal de Uberlândia - UFU, Av. João Naves de Ávila, 2121, CEP 38408-100,
Uberlândia, MG, Brasil

The composite LiFePO$_4$/polyaniline was prepared by chemical synthesis to promote the intensification of the electrochemical properties for use as cathodes in lithium ion batteries. The X-ray diffraction (XRD) of LiFePO$_4$ synthesized by solvothermal method were indexed to the orthorhombic structure, according to the JCPDS 40-1499. The spectra Raman and FTIR showed a high degree of ordering of LiFePO$_4$ with interaction between LiFePO$_4$ surface with structure conjugate of conducting polymers. The cyclic voltammogram of the composite synthesized chemically showed a significant reduction in the value of ΔE_p ($\Delta E_p = 0.20$ V) when compared to LiFePO$_4$ ($\Delta E_p = 0.41$ V), with lower charge transfer resistance values, indicating favoring electron transfer rate in the composite. Thus, the alternative synthesis route of the LiFePO$_4$ / PAni composite was easy to handle and allowed an increase in the electrochemical properties of the LiFePO$_4$, compared to the traditional methods that require additional thermal treatments.

Keywords: *solvothermal synthesis, PAni coated LiFePO$_4$, composites, cathode lithium batteries.*

1. Introduction

Currently, the demand for energy sources that are renewable and environmentally clean has driven research and the use of alternative energy sources instead of fossil fuel use. One can cite, for example, solar, wind energy, among others[1].

Most of these sources of energy is uncontrollable and / or intermittent nature, therefore, is associated with these energy sources a relatively high cost. Within this context, the lithium ions batteries are considered as one of the short-term solutions because of their high energy density and the relatively simple reaction mechanism[2].

Among the secondary energy storage devices, lithium ion stand out because they have features including: high voltage (approximately 3 V), high energy density (volumetric and mass), low self-discharge rate (2 to 8% per month) and wide operating temperature range[3]. Due to these superior features, the lithium ions batteries are widely used in various household appliances devices such as cell phones, notebooks, tablets, among others[4,5].

The transition metal oxides have been the main subject of research in the area of cathode materials for lithium ion batteries[6]. Such materials exhibit good charge storage capacity, high specific energy and excellent cycle life[7].

Classified by structure, the cathode materials include: lamellar compounds LiMO$_2$ (M = Co, Ni, Mn, etc.), spinel compounds LiM$_2$O$_4$ (M = Mn, etc.) and olivine compounds LiMPO$_4$ (M = Fe, Mn, Ni, Co, etc.)[2].

Although the lithium cobaltate (LiCoO$_2$) material has high charge capacity and high stability, increasing the battery life, the cobalt presents high cost, high toxicity and moderate reversible capacity. On the other hand, the LiMn$_2$O$_4$ presents a problem that decreases its loading capacity significantly as compared to the LiCoO$_2$. The Jahn-Teller effect occurs due to a structural anisotropic distortion in the d orbitals, from the Mn^{3+}, changing of the compact cubic symmetry to a tetragonal symmetry[8].

The LiFePO$_4$ has theoretical specific capacity (170 mA h g^{-1}) lower than that obtained for LiCoO$_2$, however it has a production cost significantly low because the iron ore reserves are relatively abundant. Regarding security, the LiFePO$_4$ does not present the problem of oxygen evolution during cycling, which is common in LiCoO$_2$ and LiMn$_2$O$_4$. This advantage is attributed to the strong covalent bond between phosphorus and oxygen, it also provides a high thermal stability material. Among the cited cathode materials, LiFePO$_4$ has lower toxicity, which, together with its low cost, enables its large-scale production[9,10].

Despite these superior characteristics, the LiFePO$_4$ has low ionic and electron conductivity at room temperature, about 10^{-5} S cm^{-1} and 10^{-10} S cm^{-1}, respectively[11,12].

Several methodologies have been employed to overcome the inherent limitations of the LiFePO$_4$, among the main can be mentioned: coating with conductive agents and anionic and cationic doping[13,14].

The conductive coating agents have been extensively used to increase the electronic conductivity of LiFePO$_4$ and hence improve its electrochemical performance. A range of conductive agents such as inorganic conductors (graphene,

carbon nanotubes, etc.), metals, conductive oxides (RuO_2, etc.), and organic conductive (conducting polymers, etc.)[15].

Conducting polymers belong to the class of conjugated polymers. They are called conjugated chains due to the fact that they show a sequence of alternating double and single bonds. Among various conducting polymers, polyaniline (PAni) is one of the most interesting in terms of its use as active component of the cathodes of lithium batteries since it has low cost, high energy density, facile synthesis and environmental friendliness. The PAni has different states oxidation and, among them, the green colored emeraldine salt has the highest conductivity (~0.1-10^2 S cm^{-1})[16]. Some papers report the improvement in the electrochemical performance of $LiFePO_4$ from the polyaniline coating, since PAni can mediate the polarity difference between the cathode and electrolyte particles, promote the permeation of electrolytes on the surface of the active particles, acting as a conducting network that connects the particles of $LiFePO_4$, diminishing, therefore, the electrical resistivity between them[17,18].

This work has as aim an alternative synthesis route of the $LiFePO_4$/PAni composite to promote an increase in the electrochemical properties of the $LiFePO_4$, favoring electron transport of the $LiFePO_4$ synthesized by solvothermal method. Then, the $LiFePO_4$/PAni composite was synthesized by chemical synthesis and its electrochemical properties as cathode material in lithium ion batteries were investigated.

2. Experimental Section

2.1 Synthesis of LiFePO₄ by solvothermal method

The $LiFePO_4$ was obtained by solvothermal synthesis using the following reagents: lithium hydroxide, ferrous sulfate heptahydrate, phosphoric acid and ethylene glycol. The molar ratio of the reactants was 3: 1: 1. Initially, 1.2×10^{-2} mol H_3PO_4 (ALDRICH, PA) and 1.2×10^{-2} mol $FeSO_4 \cdot 7H_2O$ (ALDRICH, PA) were dissolved in 40 mL of ethylene glycol. At the same time, 3.6×10^{-2} mol $LiOH \cdot H_2O$ (ACROS, PA) were dissolved in 30 mL of ethylene glycol. Subsequently, the LiOH solution was added slowly to the solution of H_3PO_4 / $FeSO_4 \cdot 7H_2O$ under constant stirring for 6 min. At the end, the mixture was placed in a reactor and heated at temperatures of 170°C, 180 °C, 190 °C and 200 °C for 10 h. The obtained precipitates were washed several times with an alcoholic solution of 50% (*V/V*) and dried at 70 °C for 8 h[19].

2.2 Chemical synthesis of the LiFePO₄/PAni composite

Initially, $LiFePO_4$ particles were dispersed in 50.0 mL of 1 mol L^{-1} H_3PO_4, containing approximately 6.25×10^{-3} mol L^{-1} (0.144 g) of sodium dodecyl sulfonate (dispersing agent).

Subsequently, the solution was placed in an ultrasound, in which it was left for 10 min for a better dispersion of the phosphate particles. 1 mol L^{-1} H_3PO_4 solution in which were added 4.1076 g (0.25 mol L^{-1}) of ammonium persulfate (oxidizing agent). The solution was cooled up to -3 °C in an ice bath containing NaCl, for better control of the polymerization kinetics of the aniline. Thereafter, it was added 1.34 mL (0.20 mol L^{-1}) of the aniline solution in the beaker. Under stirring, the oxidizing agent was added slowly. After synthesis, the solution was allowed to stand and after 48 h the solution was filtered. The dark powder was placed to dry in an oven at 80 °C for 24 h.

2.3 Microstructural characterization

2.3.1 Microstructural characterization by XRD

The structural characterization was made by X-ray diffractometry using a Shimadzu diffractometer (Model 6000, radiation Cu Kα λ = 1.5406 Å with a voltage of 40 kV, current 30 mA, at 2θ min^{-1}, from 20° to 60°. The unit cell parameters were calculated using the *Unit Cell Win* program, with the adjustment of the diffractogram peaks previously made on the *Peak Fit* software.

2.3.2 Microstructural characterization by FT-IR spectroscopy

FT-IR spectroscopy measurements were performed using an infrared spectrophotometer (ABB BOMEM MB series) using pellets of the composite powder containing KBr (1:100) from 2000 to 500 cm^{-1}.

2.3.3 Microstrutural characterization by Raman spectroscopy

Raman spectroscopy measurements were performed using a Raman spectrometer (LabRAM HR Evolution). Raman scattering spectra were performed from 2000 to 200 cm^{-1} at room temperature. The emission from a laser He-Ne ion with a wavelength of 633 nm was used. To obtain a high signal-to-noise ratio, each Raman spectrum is the average of 20 successive scans obtained at a spectral resolution of 1 cm^{-1}.

2.4 Thermal characterization by TGA

Thermogravimetric Analysis (TGA) was performed on a DTG-60H Shimadzu equipment Simultaneous DTA-TG apparatus. The heating routine occurred from room temperature (approximately 25 °C) up to 900 °C at 10 °C min^{-1} in synthetic air.

2.5 Morphological characterization by FEG

The FEG images were obtained using a Hitachi electronic scanning microscope, Model 3000, enlarging the images 80,000 times with acceleration voltage of 10 kV.

2.6 Electrochemical characterization

The electrodes were made containing 85% in mass of synthesized materials, 10% of black acetylene VULCAN XC 72-GP 2800 (CABOT USA) and 5% of Polyvinylidene Fluorite (PVDF) (ALDRICH, PA) dispersed in cyclohexanone (ALDRICH, PA). The slurry mixture was sonicated for 30 min to form a homogeneous solution. Then it was spun (5000 rpm for 5 s) on a platinum plate and, in order to evaporate the solvent, the electrodes were dried at 120 ºC for 24 h in vacuum[20].

The conventional electrochemical cell was composed of three electrodes: working electrode, as described, graphite as counter electrode and Li/Li$^+$ as the reference electrode. The electrolyte was a solution of 1.0 mol L^{-1} LiClO$_4$ in a dimethyl carbonate/ethylene carbonate (1:1 v/v) solution. The electrodes were characterized by using cyclic voltammetry in the potential range of 2.94 to 3.94 V *vs.* Li/Li$^+$ at $v = 0.1$ mV s^{-1}. All electrochemical experiments were performed in a Glove box using an Autolab PGSTAT 20 FRA, interfaced with a microcomputer using software NOVA version 1.11.

Electrochemical impedance spectroscopy (EIS) spectra were recorded by applying of alternating current (AC) amplitude of 10 mV, and the data were collected in the frequency range from 10^4 to 10^{-1} Hz.

3. Results and Discussion

3.1 Microstructural characterization by XRD of the LiFePO$_4$

Typical XRD pattern shows similarity with the standard JCPDS pattern 40-1499 indexed on basis an ortorrombic structure. The XRD pattern of LiFePO$_4$ (Figure 1) shows the presence of well resolved and highly defined peaks, thus confirming the formation of highly crystalline LiFePO$_4$ without any impurities. In the synthesis by solvothermal method is not observed the presence of peaks attributable to second
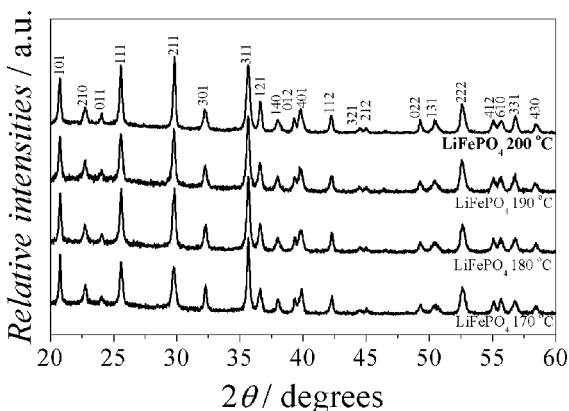
phases such as Li$_3$PO$_4$ and Fe$_3$(PO$_4$)$_2$ because the ethylene glycol acts as a weak reducing agent and minimizes the oxidation of Fe^{2+} to Fe^{3+} during synthesis of the LiFePO$_4$[17]. Besides, ethylene glycol (EG) reduced significantly the mobility rates of the different ions species (Li$^+$, Fe^{2+}) in this medium and it also acted as a soft template for facilitating the self-assembly of in situ grown nanoparticles through forming hydrogen bonds which control the crystal growth of LiFePO$_4$[21].

The unit cell parameters calculated to LiFePO$_4$ are showed in the Table 1.

There is a gradual increase of the parameters *a, b* and *c* as a function of the synthesis temperature, indicating the intercalation of lithium ions in the crystalline structure. The sample synthesized at 200 ºC presented similar parameters to the JCPDS, suggesting a stoichiometric structure. The intensity ratio between the diffraction peaks $I_{(211)}/I_{(111)}$ for LiFePO$_4$ synthesized at 190 °C and 200 °C showed higher values than others samples, as shown in Figure 2. Besides, it was noted a higher ratio between the intensity of the diffraction peaks $I_{(211)}/I_{(111)}$ (1.210) in the sample synthesized at 200 °C than those obtained at different synthesis temperatures. This higher ratio can be attributed to a probable arrangement of the LiFePO$_4$ particles due to the growth of crystals aligned in the horizontal face[19]. Then, the LiFePO$_4$ obtained at 200 ºC was used to synthesize conducting composite.

Table 1. Unit cell parameters calculated for LiFePO$_4$.

LiFePO$_4$ synthesized at	*a*(Å)	*b*(Å)	*c*(Å)	V(Å^3)
170 ºC	10.2811	5.9626	4.6814	286.9796
180 ºC	10.3202	5.9902	4.6885	289.8434
190 ºC	10.3215	5.9905	4.6943	290.2530
200 ºC	10.3328	6.0115	4.6958	291.6826
JCPDS pattern 40-1499	10.3470	6.0189	4.7039	292.9474*

*calculated from unit cell parameters *a*b*c*.

Figure 1. X-ray patterns of LiFePO$_4$ synthesized at 170 ºC, 180 ºC, 190 ºC and 200 ºC for 10 h.
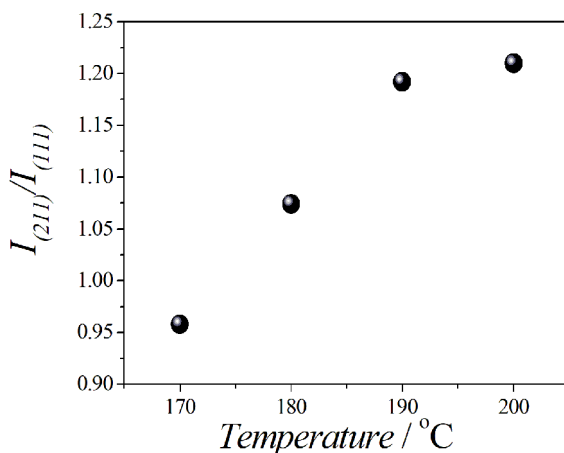

Figure 2. Ratio of intensity between (211)/(111) for the LiFePO$_4$ synthesized at 170 ºC, 180 ºC, 190 ºC and 200 ºC for 10 h.

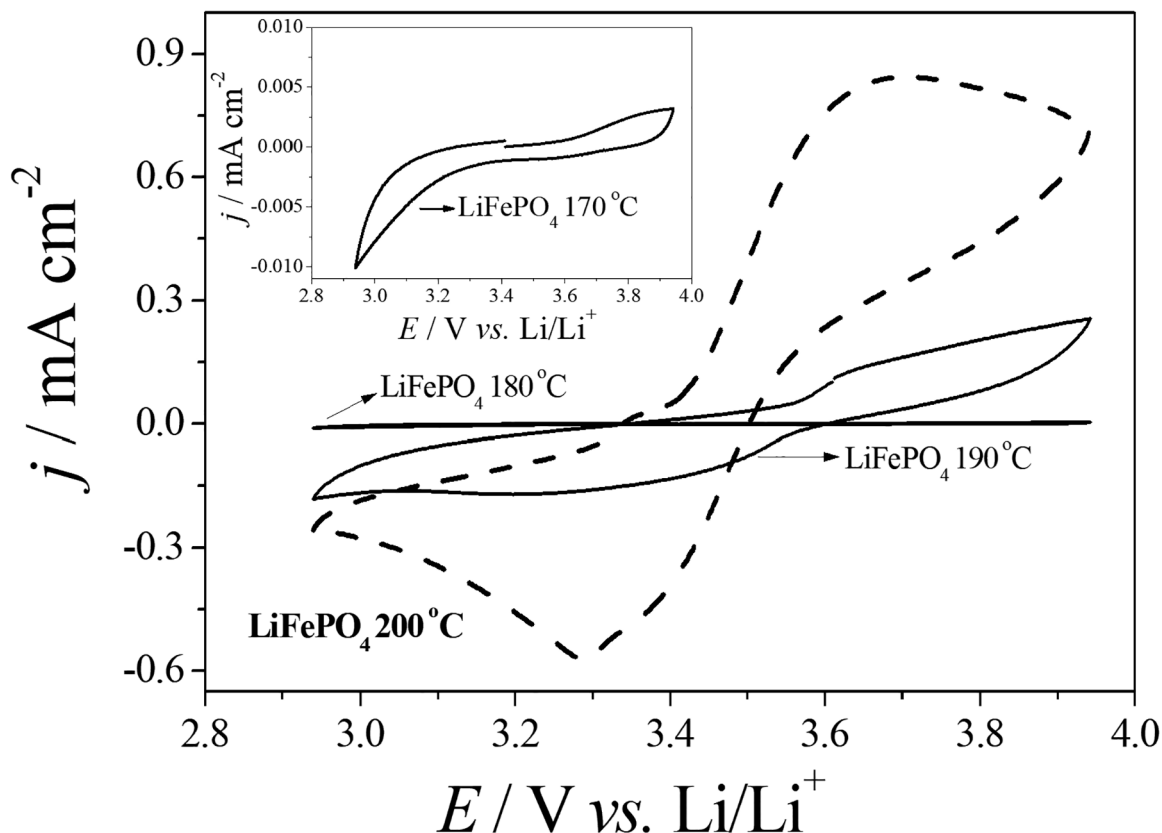**Figure 3.** Cyclic voltammograms recorded at 0.1 mV s⁻¹, in a 1.0 mol L⁻¹ LiClO₄ in EC:DMC 1:1 (*V/V*), of LiFePO₄ synthesized at 170 ºC, 180 ºC, 190 ºC and 200 ºC for 10 h. Cyclic voltammogram of LiFePO₄ synthesized at 170 ºC shown as inset.

3.2 Electrochemical characterization of the LiFePO₄

The Figure 3 shows the stabilized cyclic voltammograms (5th cycles) of the LiFePO₄ obtained at different temperatures (from 170 to 200 ºC) for 10 h by solvothermal method. The voltammetric profiles of the samples were similar to those obtained for stoichiometric LiFePO₄, showing that the redox processes occur in one stage, at corresponding to the deintercalation/intercalation of lithium ion in the $Li_x FePO_4$ structure ($0 \leq x \leq 1$) in the octahedral sites[12]. In the voltammogram of the LiFePO₄ (at 200 ºC) is showed defined redox peaks and more intense than those obtained for the LiFePO₄ obtained at 190 ºC. In this last, it is observed a transition of Fe^{2+} to Fe^{3+} at 3.67 V *vs*. Li/Li⁺, and the reducing process of the Fe^{3+} to Fe^{2+} (3.27 V *vs*. Li/Li⁺). The LiFePO₄ synthesized at 170 and 180 ºC did not present electrochemistry activity.

The difference in sample responses is associated with the fact that possibly in the samples synthesized at 190 °C and 200 °C, the preferred diffusion axis (010) has been decreased. This explanation can be based on the intensity of the diffraction peaks $I_{(211)}/I_{(111)}$, being attributed to a probable arrangement of the LiFePO₄ particles due to the growth of crystals aligned in the horizontal face[19], which may favor lithium ion transport.

3.3 Microstructural characterization by FTIR

In order to obtain information about molecular structure of materials, the LiFePO₄/PAni composite and its constituent materials were characterized by FTIR spectral range of 2000-500 cm⁻¹. In the FTIR spectra of the LiFePO₄ (Figure 4), bands were observed in the region of 1139-500 cm⁻¹ corresponding to the internal intramolecular vibration modes arising from
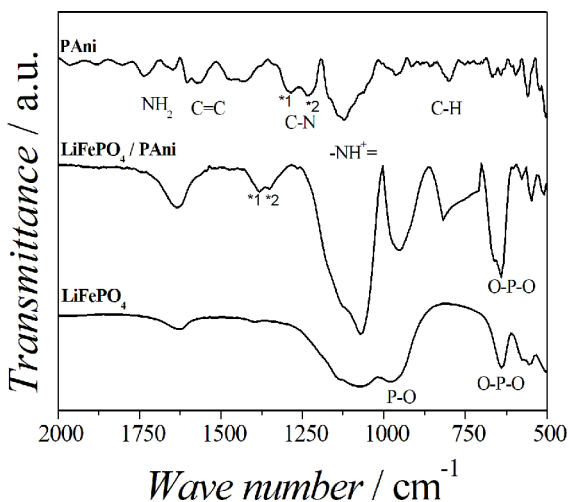

Figure 4. FTIR spectra of LiFePO₄, PAni and LiFePO₄/PAni.

the $(PO_4)^{3-}$. In the region of 647-500 cm⁻¹ is observed bands attributed to bending modes (v_2 and v_4) of asymmetric and symmetric O-P-O links as well as vibrations of lithium ions[22]. The bands present in the range of 945-1139 cm⁻¹ correspond to symmetric and asymmetric stretching modes (v_1 and v_3) PO bond. The band at 547 cm⁻¹ corresponds to the vibration of lithium ions in the octahedral sites of the PO_4^{3-}. Moreover, it was not observed any other vibrational bands that are associated with Li_3PO_4, P_2O_7 or P_3O_{10}, which reflects the absence of the secondary phases in the $LiFePO_4$.

In the FTIR spectrum obtained for PAni and $LiFePO_4$ / PAni can observe the presence of a band around 1130 cm⁻¹, which is known in the literature as an "electronic band" being associated, so the doped form of polyaniline, more specifically the vibration mode the structures -NH⁺=[23]. Moreover, it is observed for the $LiFePO_4$ / PAni there is inverse relationship intensity in 1382-1354 cm⁻¹ (*1 and *2) compared with polyaniline, revealing that the polyaniline in the composite is richer in quinoid units than the PAni pure, probably because the chain of polyaniline deposited on the surface of the $LiFePO_4$ has a greater conjugation[24].

The band corresponding to C-H out of plane deformation due to the presence of mono-substituted benzene rings was observed, indicating the high degree of polymerization in the composite (Figure 4). This interpretation is also supported by the presence, in both materials, a band around 1300 cm⁻¹, which is often associated with the C-N stretch aromatic secondary amine groups[25]. The band observed at around 1232 cm⁻¹ can be assigned to CN stretching vibration of benzoic species[26].

3.4 Microstructural characterization by Raman spectroscopy

In order to obtain information about molecular structure of materials, the $LiFePO_4$/PAni composite and its constituent materials were characterized by Raman spectroscopy. The Figure 5 shows the Raman spectra of $LiFePO_4$, PAni and $LiFePO_4$/ PAni obtained in the spectral range from 2000 to 200 cm⁻¹.

The characteristic vibrations of $LiFePO_4$ are observed below 1200 cm⁻¹ and the bands of $LiFePO_4$ can be divided into two classes: internal and external optic modes. The internal modes are located above 400 cm⁻¹ and are originate from the intramolecular vibrations of the PO_4^{3-} anion. The external modes are primarily composed of translatory and vibrational motions of the PO_4^{3-} ions and translatory motion of the Fe^{2+} ions[27]. Moreover, the intense symmetric stretching band at 949 cm⁻¹ can be identified as well as the asymmetric stretching bands at 995 and 1067 cm⁻¹ indicating non-distorted PO_4^{3-}[27]. Furthermore, no evidence of secondary phases such as iron oxide was seen in the Raman spectra, in accordance with the XRD data.

The Raman spectra of PAni and $LiFePO_4$/PAni (Figure 5) show the all characteristic bands of PAni. The bands near

1500 cm⁻¹ and 1600 cm⁻¹ are assigned mainly to the benzenoid C-C ring stretching vibration and the quinoid C-C stretching mode, respectively. The band located at 1338 is atributed to C-N⁺ vibrations, indicating that the polyaniline is in the doped state. The band around 1168 cm⁻¹ is attributable to the out-of-plane-C-H bending. Moreover, the band around 575 cm⁻¹ assigned to cross linking between PAni chains[28]. It should be noted that the bands present small shifts in the $LiFePO_4$ / PAni spectrum when compared to the PAni spectrum, which should be associated to an chemical interaction of Pani with $LiFePO_4$.

3.5 Thermal characterization by TGA

The composite $LiFePO_4$/PAni and its constituent materials were characterized by Thermogravimetric analysis (TGA) in synthetic air in order to determine the percentage of polyaniline in the composite as well as verify the percentage of Fe^{2+} in $LiFePO_4$ and the mass loss levels of materials (Figure 6).

The TGA curve $LiFePO_4$ shows a small increase in mass at 300 °C which is attributed to the Fe^{2+} oxidation in air and it can be represented by Equation 1[29,30].
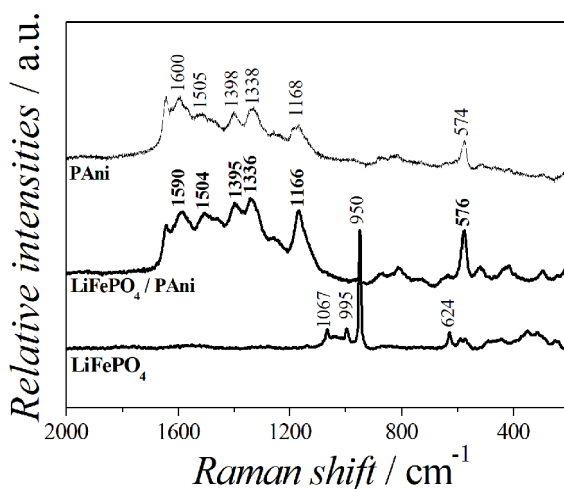

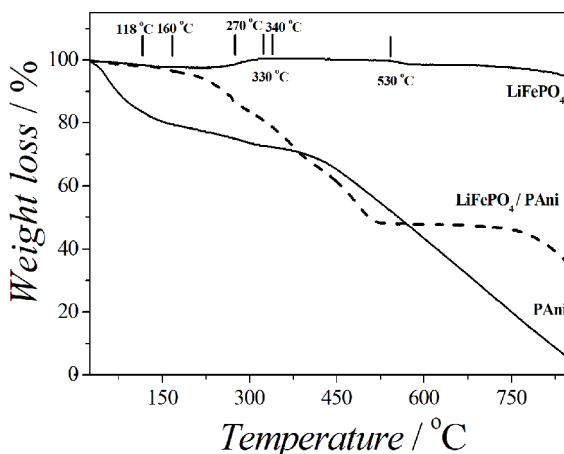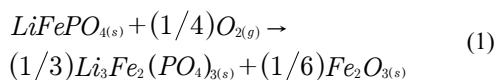**Figure 5.** Raman spectra of $LiFePO_4$, PAni and $LiFePO_4$/PAni.

Figure 6. TGA of $LiFePO_4$, PAni and $LiFePO_4$/PAni, in synthetic air.

$$LiFePO_{4(s)} + (1/4)O_{2(g)} \rightarrow$$
$$(1/3)Li_3Fe_2(PO_4)_{3(s)} + (1/6)Fe_2O_{3(s)} \qquad (1)$$

In the TGA curve of PAni was observed three stages of weight loss below 850 °C. The first stage weight loss in the range 33-118 °C can be attributed to water molecules strongly bound to the polymers and will probably not have been removed. The second mass loss stage ranges 160-270 °C, it was assigned to the elimination of dopant anions (dihidrogen phosphate present in the electrolyte) and the last stage 340-850 °C is attributed to the thermal decomposition of polymer chains[31]. At the end of the analysis there was not residue of the analyzed conductive polymer.

For the LiFePO$_4$/PAni composite, there was a weight loss in the range 40-200 °C and 215-290 °C attributed to evaporation of water and elimination of dopant anions, respectively. A weight loss at 330-520 °C corresponds to the thermal decomposition of the polyaniline chains and leaving a residue of approximately 44% weight, corresponding to the Li$_3$Fe$_2$(PO$_4$)$_3$ and Fe$_2$O$_3$ (Table 2).

3.6 Morphological characterization by FEG

The FEG micrographs shown in the Figure 7 (a) and (b) were further analyzed with the *Image J* software, which allowed counting the amount and measuring the size (d) of the particles. The amount of particles considered for the counting was equal to 100; to ensure reliability, this counting was done on five different micrographs of each material. The thus obtained average particle size distributions are shown in Fig. 7 (c).

It is observed that both LiFePO$_4$ and LiFePO$_4$ / PAni presented a morphology in the shape of plates which size varied from 0.2 to 1.2 μm (Fig. 7). The polyaniline, on the other hand, presents a porous morphology, covering the particles of LiFePO$_4$ and allowing the intercalation of lithium ions on the surface of LiFePO$_4$. Thus, we infer that both materials, LiFePO$_4$ and LiFePO$_4$/PAni composite, present particle sizes of nanometric scale, suggesting polymer thin film in the surface LiFePO$_4$.

3.7 Electrochemical characterization of LiFePO$_4$ / PAni composite and their constituent materials

In order to obtain information on the electrochemical activity of the materials as well as to verify the influence of PAni on the electrochemical properties of the LiFePO$_4$, the LiFePO$_4$ / PAni composite and its constituent materials were characterized by cyclic voltammetry. The Figure 7 shows the cyclic voltammograms of LiFePO$_4$, PAni and LiFePO$_4$ / PAni. In the voltammogram of the LiFePO$_4$ (at 200 ºC) is showed defined redox peaks and more intense than those obtained for the LiFePO$_4$ obtained at 190 ºC. In this last, it is observed a transition of Fe^{2+} to Fe^{3+} at 3.67 V *vs.* Li/Li$^+$, and the reducing process of the Fe^{3+} to Fe^{2+} (3.27 V *vs.* Li/Li$^+$). The LiFePO$_4$ synthesized at 170 ºC did not present electrochemistry activity.

In the voltammogram of PAni the profile is predominantly capacitive. In voltammogram of the LiFePO$_4$/PAni composite was observed the same well defined redox peaks associated oxidation of Fe^{2+} to Fe^{3+} and reducing of Fe^{3+} to Fe^{2+} at 3.61 and 3.42 V, respectively (Figure 8). However, in this voltammogram a current density is higher than that obtained for pure PAni. Besides, it is noteworthy that the distance between the oxidation and reduction peaks ($\Delta E_p = 0.20$ V) is significantly lower when compared to LiFePO$_4$ ($\Delta E_p = 0.41$ V).

This is due to the fact that the composite material has a more reversible redox process as compared to pure LiFePO$_4$, therefore the PAni contributes effectively to the electronic conductivity of the composite material. It was observed a significant improvement of the redox reversibility of the LiFePO$_4$ with the use of other conductive agents such as: carbon, graphene, etc;[19,32] as shown in Table 3.

Table 2. Temperatures values of thermal events for LiFePO$_4$, PAni and LiFePO$_4$/PAni.

Material	Event temperature (ºC)	Change mass (%)	Thermal event assignment
LiFePO$_4$	300-800	+5	Oxidation of LiFePO$_4$
PAni	33-118	-14	Removal of adsorbed water
	160-270	-12	Elimination of dopant anion
	350-850	-72	Thermal decomposition of polymer chains
LiFePO$_4$/PAni	40-200	-12	Removal of adsorbed water
	215-290	-8	Elimination of dopant anion
	330-530	-36	Thermal decomposition of polymer chains

Table 3. Values of oxidation and reducing potential vs. Li/Li$^+$ for LiFePO$_4$ and LiFePO$_4$/PAni.

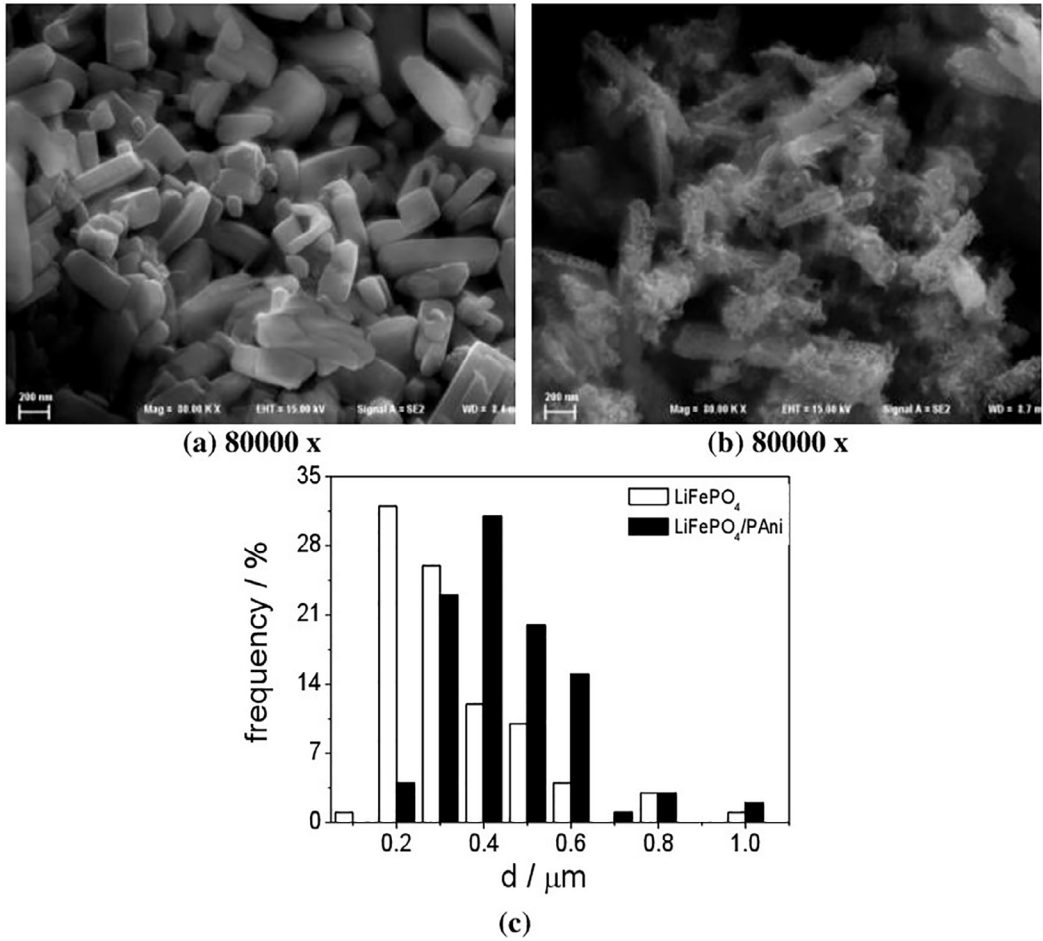| Material	$E_{ox.}$ (V *vs.* Li/Li$^+$)	$E_{red.}$ (V *vs.* Li/Li$^+$)	$\Delta(E_{ox.} - E_{red.})$ (V *vs.* Li/Li$^+$)	Reference
LiFePO$_4$	3.69	3.28	0.41	This work
LiFePO$_4$(solid state reaction)	~3.90	~3.10	0.80	[30]
LiFePO$_4$/PAni	3.61	3.42	0.19	This work
LiFePO$_4$/C (solid state reaction)	~3.80	~3.40	0.40	[30]

(a) 80000 x **(b) 80000 x**

(c)

Figure 7. FEG micrographs of: (a) LiFePO$_4$ and (b) LiFePO$_4$/PAni; (c) Average (n = 5) particle size distribution for the LiFePO$_4$ and LiFePO$_4$/PAni.
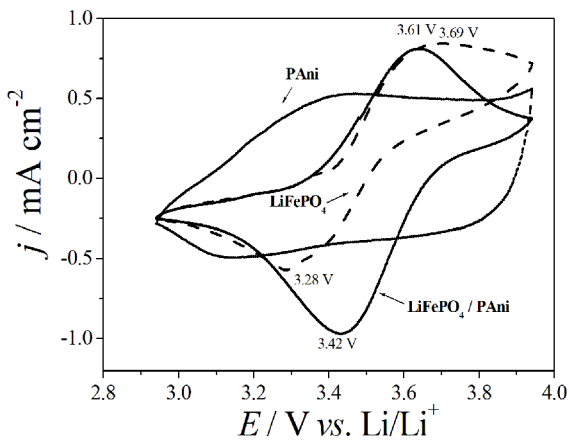

Figure 8. Cyclic voltammograms recorded at 0.1 mV s^{-1}, in a 1.0 mol L^{-1} LiClO$_4$ in EC:DMC 1:1 (*V/V*), of LiFePO$_4$ synthesized at 200 °C for 10 h, of PAni and LiFePO$_4$/PAni.

3.8 Electrochemical impedance of LiFePO$_4$ /PAni composite and their constituent materials

It was evaluated the electrical resistance of the films as well as the influence of polyaniline on the electrical conductivity of the LiFePO$_4$ film.

In the Nyquist plots (Z" *vs.* Z') of the PAni (Figure 9) it is observed a semi-circle in the region of high frequencies and by extrapolating towards the real axis impedance obtained the charge transfer resistance values (R_{ct}) corresponding to the electrical resistance on the film / electrode interface. The region of intermediate frequencies at low a linear relationship with slope of about 45 degrees corresponding to the diffusion of ionic species in the electrolyte toward to the polymeric film.

Although the Nyquist plot of LiFePO$_4$ / PAni shows a similar profile to the PAni plot, a reduction of the diameter of the semicircle is observed, which indicates a significant decreased charge transfer resistance. The R_{ct} values were 50 and 14 Ω cm^2 for PAni and LiFePO$_4$/PAni, respectively (Table 4).

In the Nyquist plot of LiFePO$_4$ observed predominance of the diffusion process that is attributed to the lithium insertion and of the ions in the structure of the material.

Obviously, the LiFePO$_4$/PAni has the smallest R_{ct}, indicating that the polyaniline coating improves the electron transfer kinetics as already explained, the polymer chains of polyaniline form conductive networks that interconnect the
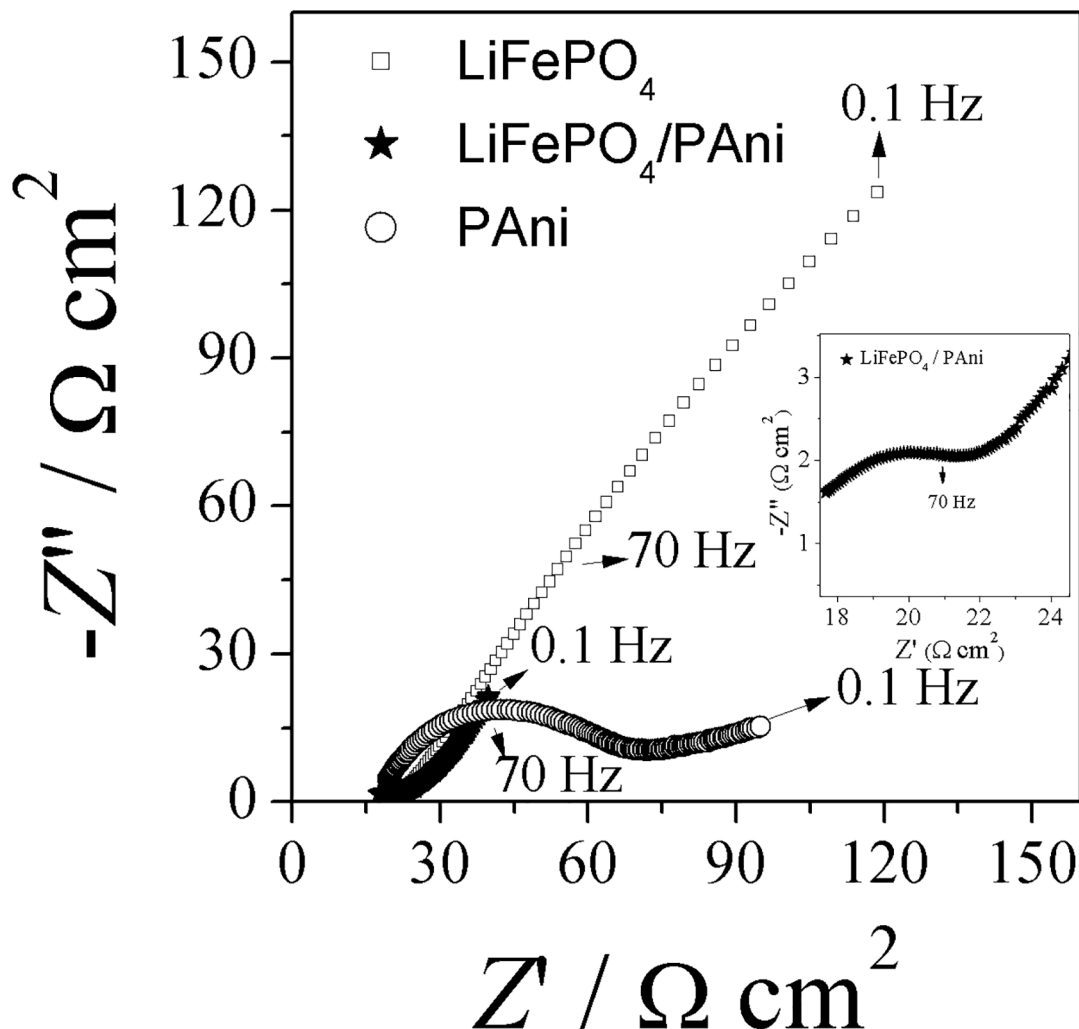
Figure 9. Nyquist diagrams of LiFePO$_4$, PAni and LiFePO$_4$/PAni, in a 1.0 mol L^{-1} LiClO$_4$ in EC:DMC 1:1 (*V/V*), in the range 10^4 to 10^{-1} Hz to open circuit potential. High frequency region in Nyquist diagram of LiFePO$_4$/PAni is shown as inset.

Table 4. Electrochemical parameters of the PAni and LiFePO$_4$/PAni.

Material	*R*ct (Ω cm²)	*R*s (Ω cm²)	*C*dc (µF)
PAni	50.00	18.13	60.13
LiFePO$_4$/ PAni	14.00	19.00	47.72

LiFePO$_4$ particles, increasing the electronic conductivity of the composite and it can significantly improve the charge transfer reaction[18,29].

4. Conclusions

The solvothermal method at low temperature was used to synthesize the LiFePO$_4$ with high crystallinity and free from secondary phases. The alternative synthesis route of the LiFePO$_4$/PAni composite was easy to handle and allowed an improvement in the electrochemical properties of the LiFePO$_4$, compared to the traditional methods that require additional thermal treatments. The ratio of the constituents in composite materials of LiFePO$_4$/PAni was 44% to the oxide and 56% to the polyaniline. Raman spectrum of the composite showed a possible chemical interaction between LiFePO$_4$ surface and structure conjugate of conducting polymers. The cyclic voltammogram of LiFePO$_4$/PAni composite presented a predominant faradaic profile and a lower value of ΔE_p compared to the LiFePO$_4$. The charge transfer resistance to the composite was lower than the obtained for its constituent materials, indicating favoring electron transfer rate in the composite. Therefore, the synthesis of LiFePO$_4$ by solvothermal method as well as the synthesis of

the LiFePO₄/PAni composite were effective approaches to overcome the problem of low ionic and electronic conductivity of the LiFePO₄ and thus becoming a promising material as cathode in lithium ion batteries.

5. Acknowledgments

6. References

1. Lewis NS, Nocera DG. Powering the planet: Chemical challenges in solar energy utilization. *Proceedings of the National Academy of Science of the United States of America*. 2006;103(43):15729-15735.

2. Xu B, Qian D, Wang Z, Meng YS. Recent progress in cathode materials research for advanced lithium ion batteries. *Material Science and Engineering: R: Reports*. 2012;73(5-6):51-65.

3. Linden D, Reddy TB, eds. *Handbook of Batteries*. New York: McGraw-Hill; 2005.

4. Tarascon JM, Armand M. Issues and challenges facing rechargeable lithium batteries. *Nature*. 2011;414:359-367.

5. Wang G, Xie J, Wu C, Zhang S, Cao G, Zhao X. Submicron lithium nickel manganese oxide spinel with long cycling stability and high rate performance prepared by facile route. *Journal of Power Sources*. 2014;265:118-124.

6. Xia H, Luo Z, Xie J. Nanostructured LiMn₂O₄ and their composites as high performance cathodes for lithium-ion batteries. *Progress in Natural Science: Materials International*. 2012;22(6):572-584.

7. Schoonman J, Tuller HL, Kelder EM. Defect chemical aspects of lithium-ion battery cathodes. *Journal of Power Sources*. 1999;81-82:44-48.

8. Shin Y, Manthiram A. Factors Influencing the Capacity Fade of Spinel Lithium Manganese Oxides. *Journal of the Electrochemical Society*. 2004;151(2):A204-A208.

9. Hong KS, Yu SM, Ha MG, Ahn CW, Hong TE, Jin JS, et al. Preparation of LiFePO₄ Using Chitosan and its Cathodic Properties for Rechargeable Li-Ion Batteries. *Bulletin of the Korean Chemical Society*. 2009;30(8):1719-1723.

10. Julien CM, Zaghib K, Mauger A, Groult H. Enhanced Electrochemical Properties of LiFePO₄ as Positive Electrode of Li-ion Batteries for HEV Application. *Advances in Chemical Engineering and Science*. 2012;2(3):321-329.

11. Andersson AS, Kalska B, Häggström L, Thomas JO. Lithium extraction/insertion in LiFePO₄: an X-ray diffraction and Mössbauer spectroscopy study. *Solid States Ionics*. 2000;130(1-2):41-52.

12. Padhi AK, Nanjundaswamy KS, Goodenough JB. Phospho-olivines as Positive-Electrode Materials for Rechargeable Lithium Batteries. *Journal of the Electrochemical Society*. 1997;144(4):1188-1194.

13. Prosini PP. *Iron Phosphate Materials as Cathodes for Lithium Batteries: The Use of Environmentally Friendly Iron In Lithium Batteries*. New York: Springer-Verlag; 2011.

14. Zaghib K, Mauger A, Julien CM. Overview of olivines in lithium batteries for green transportation and energy storage. *Journal of Solid State Electrochemistry*. 2012;16(3):835-845.

15. Ding B. *High Performance Nanostructured Phospho-Olivine Cathodes for Llithium-ion Batteries*. [Thesis]. Singapore: National University of Singapore; 2014.

16. Zoppi RA, De Paoli MA. Aplicações Tecnológicas de Polímeros Intrinsicamente Condutores: Perspectivas Atuais. *Química Nova*. 1993;16(6):560-569.

17. Chen WM, Qie L, Yuan LX, Xia SA, Hu XL, Zhang WX, et al. Insight into the improvement of rate capability and cyclability in LiFePO₄/polyaniline composite cathode. *Electrochimica Acta*. 2011;56(6):2689-2695.

18. Posudievsky OY, Kozarenko OA, Dyadyun VS, Koshechko VG, Pokhodenko VD. Advanced electrochemical performance of hybrid nanocomposites based on LiFePO₄ and lithium salt doped polyaniline. *Journal of Solid State Electrochemistry*. 2015;19(9):2733-2740.

19. Nan C, Lu J, Chen C, Peng Q, Li Y. Solvothermal synthesis of lithium iron phosphate nanoplates. *Journal of Materials Chemistry*. 2011;21(27):9994-9996.

20. Amaral FA, Santana LK, Campos IO, Fagundes WS, Xavier FFS, Canobre SC. Pechini Synthesis of Nanostructured Li₁.₀₅M₀.₀₂Mn₁.₉₈O₄ (M = Al³⁺ or Ga³⁺). *Materials Research*. 2015;18(Suppl 2):250-259.

21. Saravanan K, Reddy MV, Balaya P, Gong H, Chowdari BVR, Vittal JJ. Storage performance of LiFePO₄ nanoplates. *Journal of Materials Chemistry*. 2009;19(5):605-610.

22. Shahid R, Murugavel S. Synthesis and characterization of olivine phosphate cathode material with different particle sizes for rechargeable lithium-ion batteries. *Materials Chemistry and Physics*. 2013;140(2-3):659-664.

23. Neoh KG, Kang ET, Tan KL. Evolution of polyaniline structure during synthesis. *Polymer*. 1993;34(18):3921-3928.

24. Nagaraja M, Mahesh HM, Manjanna J, Rajanna K, Kurian MZ, Lokesh SV. Effect of Multiwall Carbon Nanotubes on Electrical and Structural Properties of Polyaniline. *Journal of Electronic Materials*. 2012;41(7):1882-1885.

25. Ryu KS, Moon BW, Joo J, Chang SH. Characterization of highly conducting lithium salt doped polyaniline films prepared from polymer solution. *Polymer*. 2001;42(23):9355-9360.

26. Quillard S, Louarn G, Lefrant S, Macdiarmid AG. Vibrational analysis of polyaniline: A comparative study of leucoemeraldine, emeraldine, and pernigraniline bases. *Physical Review B: Condensed Matter*. 1994;50(17):12496-12508.

27. Faques-Ledent MT, Tarte P. Vibrational studies of olivine-type compounds-II orthophosphates, -arsenates and -vanadates AᵢBᵢᵢXVO₄. *Spectrochimica Acta Part A: Molecular Spectroscopy*. 1974;30(3):673-689.

28. Zhang L, Wan M. Polyaniline/TiO₂ Composite Nanotubes. *The Journal of Physical Chemistry B*. 2003;107(28):6748-6753.

29. Gong C, Deng F, Tsui CP, Xue Z, Ye YS, Tang CY, et al. PAni-PEG copolymer modified LiFePO$_4$ as a cathode material for high-performance lithium ion batteries. *Journal of Materials Chemistry A*. 2014;2(45):19315-19323.

30. Yim CH, Baranova EA, Abu-Lebdeh Y, Davidson I. Highly ordered LiFePO$_4$ cathode material for Li-ion batteries templated by surfactant-modified polystyrene colloidal crystals. *Journal of Power Sources*. 2012;205:414-419.

31. Bekri-Abbes I, Srasra E. Solid-state synthesis and electrical properties of polyaniline/Cu-montmorillonite nanocomposite. *Materials Research Bulletin*. 2010;45(12):1941-1947.

32. Kumar A, Thomas R, Karan NK, Saavedra-Arias JJ, Singh MK, Majumber SB, et al. Structural and Electrochemical Characterization of Pure LiFePO$_4$ and Nanocomposite C-LiFePO$_4$ Cathodes for Lithium Ion Rechargeable Batteries. *Journal of Nanotechnology*. 2009;2009:176517.